

# Impact-based Skill Evaluation of Seasonal Precipitation Forecasts

Zahir Nikraftar<sup>1</sup>, Rendani Mbuva<sup>1</sup>, Mojtaba Sadegh<sup>2</sup>, and Willem Adolf Landman<sup>3</sup>

<sup>1</sup>Queen Mary University of London

<sup>2</sup>Boise State University

<sup>3</sup>Council for Scientific and Industrial Research

December 27, 2023

## Abstract

Forecasting hydroclimatic extremes holds significant importance considering the increasing trends in natural cascading climate-induced hazards such as wildfires, floods, and droughts. This study evaluates the performance of five Copernicus Climate Change Service (C3S) seasonal forecast models (i.e., CMCC, DWD, ECCO, UK-Met, and Météo-France) in predicting extreme precipitation events from 1993 to 2016 using 28 extreme precipitation indices reflecting timing and intensity of precipitation in a seasonal timescale. We design indices using various precipitation thresholds to reflect model skill in capturing the distribution and intensity of precipitation over a season. We use percentage bias, the Kendall Tau rank correlation, and ROC scores for skill evaluation. We introduce an impact-based framework to evaluate model skill in capturing extreme events over regions prone to natural disasters such as floods and wildfires. The performance of models varies across regions and seasons. The model skill is highlighted primarily in the tropical and inter-tropical regions, while skill in extra-tropical regions is markedly lower. Elevated precipitation thresholds correlate with heightened model bias, revealing deficiencies in modelling severe precipitation events. The impact-based framework analysis highlights the superior predictive capabilities of the UK-Met and Météo-France models for extreme event forecasting across many regions and seasons. In contrast, other models exhibit strong performance in specific regions and seasons. These results advance our understanding of an impact-based framework in capturing a broad spectrum of extreme climatic events through the strategic amalgamation of diverse models across different regions and seasons, offering valuable insights for disaster management and risk analysis.

## Hosted file

979728\_0\_art\_file\_11667169\_s54qy2.docx available at <https://authorea.com/users/708832/articles/693177-impact-based-skill-evaluation-of-seasonal-precipitation-forecasts>

## Hosted file

979728\_0\_supp\_11597974\_s4zcgk.docx available at <https://authorea.com/users/708832/articles/693177-impact-based-skill-evaluation-of-seasonal-precipitation-forecasts>

# Impact-based Skill Evaluation of Seasonal Precipitation Forecasts

Zahir Nikraftar<sup>1</sup>, Rendani Mbuva<sup>1,2</sup>, Mojtaba Sadegh<sup>3,4</sup>, Willem A. Landman<sup>5</sup>

<sup>1</sup> Machine Intelligence and Decision Systems (MInDS) Research Group, School of Electronic Engineering and Computer Science, Queen Mary University of London (QMUL), London, UK, E1 4NS.

<sup>2</sup> School of Statistics and Actuarial Science, University of Witwatersrand, Johannesburg, South Africa

<sup>3</sup> Department of Civil Engineering, Boise State University, Boise, ID, USA.

<sup>4</sup> United Nations University Institute for Water, Environment and Health, Hamilton, ON, Canada.

<sup>5</sup> Department of Geography, Geoinformatics and Meteorology, University of Pretoria, Pretoria, South Africa.

Corresponding Author: Rendani Mbuva ([r.mbuva@qmul.ac.uk](mailto:r.mbuva@qmul.ac.uk))

## Abstract

Forecasting hydroclimatic extremes holds significant importance considering the increasing trends in natural cascading climate-induced hazards such as wildfires, floods, and droughts. This study evaluates the performance of five Copernicus Climate Change Service (C3S) seasonal forecast models (i.e., CMCC, DWD, ECCO, UK-Met, and Météo-France) in predicting extreme precipitation events from 1993 to 2016 using 28 extreme precipitation indices reflecting timing and intensity of precipitation in a seasonal timescale. We design indices using various precipitation thresholds to reflect model skill in capturing the distribution and intensity of precipitation over a season. We use percentage bias, the Kendall Tau rank correlation, and ROC scores for skill evaluation. We introduce an impact-based framework to evaluate model skill in capturing extreme events over regions prone to natural disasters such as floods and wildfires. The performance of models varies across regions and seasons. The model skill is highlighted primarily in the tropical and inter-tropical regions, while skill in extra-tropical regions is markedly lower. Elevated precipitation thresholds correlate with heightened model bias, revealing deficiencies in modelling severe precipitation events. The impact-based framework analysis highlights the superior predictive capabilities of the UK-Met and Météo-France models for extreme event forecasting across many regions and seasons. In contrast, other models exhibit strong performance in specific regions and seasons. These results advance our understanding of an impact-based framework in capturing a broad spectrum of extreme climatic events through the strategic amalgamation of diverse models across different regions and seasons, offering valuable insights for disaster management and risk analysis.

## Key Points

- The C3S models' skill in predicting precipitation variability across seasons is highlighted in the tropical and inter-tropical regions.
- UK-Met and Météo-France consistently outperform other models, demonstrating better accuracy and reliability, aligning with findings from previous studies.

- 45 • An Impact-Based framework offers valuable insights for targeted risk assessments,  
46 particularly in regions prone to wildfire and floods.

47

## 48 **Plain Language Summary**

49

50 This study looks at how well five seasonal forecast models can predict extreme precipitation  
51 and related events such as floods and droughts. We assess the performance of models by  
52 looking at 28 different extreme precipitation indices that show when and how much it rains  
53 during different seasons. The results show that some models do better in certain areas and  
54 seasons. The study also introduces a new way of assessing model skill by looking at the  
55 impact of extreme events in areas prone to disasters such as floods and wildfires. We find that  
56 two models, UK-Met and Météo-France, are particularly good at predicting extreme events in  
57 various places and seasons. This information is important for better managing and  
58 understanding the risks of natural disasters.

59

60

### 61 **1. Introduction**

62

63 Precipitation plays a crucial role in momentum flux exchange at the ocean– atmosphere-land  
64 interface (Xue et al., 2020), and as such, is one of the primary outputs of weather and climate  
65 models (Tapiador et al., 2019). Numerous international initiatives such as the North  
66 American Multi-Model Ensemble (NMME)<sup>1</sup> and Copernicus Climate Change Service (C3S)<sup>2</sup>  
67 multi-system seasonal forecast predict precipitation, and other Météorological factors, at  
68 various spatiotemporal scales. Such forecasts are used for a variety of purposes, including  
69 extreme event early warning. Forecast models rely on the sources of atmospheric  
70 predictability, such as modes of variability including El Niño–Southern Oscillation (ENSO),  
71 Madden–Julian oscillation (MJO), Quasi-Biennial Oscillation (QBO), and Indian Ocean  
72 Dipole (IOD). Other sources of predictability include anomalies in the initial state of an Earth  
73 system component with a persistence time that aligns with the projected forecast duration  
74 (i.e., large-scale anomalies in upper ocean heat content, sea ice, snowpack, soil moisture), and  
75 external forcing (Assessment of Intraseasonal to Interannual Climate Prediction and  
76 Predictability, 2010; Baldwin et al., 2003; Committee on Developing a U.S. Research  
77 Agenda to Advance Subseasonal to Seasonal Forecasting et al., 2016; Lau & Waliser, 2012;  
78 Shukla et al., 2000; Zhang et al., 1997). Despite the significance of precipitation, numerical  
79 weather models face difficulties in predicting its spatial patterns, timing and intensity  
80 (Tapiador et al., 2019; Mallakpour et al. 2022). This is because the predictive capabilities of  
81 seasonal forecast models are constrained by the uncertainty in initial and boundary  
82 conditions, climate change-induced modifications of teleconnection patterns, imperfect  
83 parameterization schemes, and the variability in parameters (Villarini et al., 2011; Xu et al.,  
84 2021).

---

<sup>1</sup> <https://www.cpc.ncep.noaa.gov/products/NMME/>

<sup>2</sup> <https://cds.climate.copernicus.eu/>

85

86 Accurate precipitation predictions are of great importance in the formulation of mitigation  
87 and adaptation measures for climate and hydrological extreme events as well as minimizing  
88 impacts from their cascading hazards such as flood, drought, and wildfire (Gebrechorkos et  
89 al., 2022; Vitart & Robertson, 2018). Recently several environmental and Climate  
90 Forecasting Systems such as the hydrological forecasting system, the Canadian Forest Fire  
91 Weather Index System<sup>3</sup>, and the global drought forecasting system<sup>4</sup> have been developed,  
92 which use seasonal forecasts as input with the purpose of weather extremes risk assessment  
93 and response (Alfieri et al., 2013; Arheimer et al., 2020; Samaniego et al., 2019; Thielen et  
94 al., 2009). The accuracy and trustworthiness of such systems is highly dependent on the  
95 process representation and parametric accuracy of the weather forecast models that provide  
96 the forcing for risk assessment (Gebrechorkos et al., 2022; Wanders & Wood, 2016). The  
97 skill of seasonal forecast systems has a substantial spatial variability which could be due to  
98 factors like quality of observation systems, model biases, and inherent properties of the  
99 climate system (Kumar & Zhu, 2018). Also, seasonal forecast performance can vary spatially  
100 across regions due to the complex and region-specific interactions between climate drivers  
101 and local environmental factors (Hao et al., 2018). Therefore, it is essential to assess the  
102 performance of different forecasting models across diverse global regions, and specific to the  
103 impacts that forecast errors may induce to identify most the effective and reliable models.

104

105 While studies have evaluated the skill of seasonal forecast models in predicting total  
106 precipitation at the sub seasonal to seasonal scales (Becker et al., 2014; Gebrechorkos et al.,  
107 2022; Nobakht et al., 2021; Roy et al., 2020), there is a need for an alternative impact-based  
108 assessment of forecast models that can inform their applicability for specific target extremes  
109 (e.g., flood, wildfire). Traditional forecast model performance assessments conduct a top-  
110 down hazard information approach by mainly investigating the model's skill in capturing  
111 weather patterns in comparison to the reference datasets (De Andrade et al., 2019; Moron &  
112 Robertson, 2020; Vitart & Robertson, 2018). The shift towards impact-based assessment  
113 framework reflects the evolving landscape of climate science and its increasing relevance in  
114 the face of a changing climate (Rad et al. 2022). It emphasizes the importance of moving  
115 beyond traditional evaluation methods and towards a comprehensive understanding of how  
116 weather forecasts directly influence society, ecosystems, and infrastructure resilience  
117 (AghaKouchak et al., 2018; Khorshidi et al., 2020; Mallakpour et al., 2022; Modaresi Rad et  
118 al., 2022; Sadegh et al., 2018). Such a framework considers the vulnerability of the local  
119 environment to specific weather events and warns of the associated impacts. An instance of  
120 such an influence might involve a chain reaction of hazards, like flooding due to repeated  
121 heavy rainfall events (Sadegh et al. 2018) or wildfires resulting from consecutive days of no  
122 precipitation and increased temperature, which can create conditions conducive to ignition  
123 (Khorshidi et al. 2020). Impact-based assessment of seasonal precipitation forecasts involve  
124 assessing the effectiveness of models by considering the real-world impact of extreme

---

<sup>3</sup> [http://cwfis.cfs.nrcan.gc.ca/en\\_CA/background/summary/fdr](http://cwfis.cfs.nrcan.gc.ca/en_CA/background/summary/fdr)

<sup>4</sup> [http://iridl.ldeo.columbia.edu/maproom/Global/Drought/Global/CPC\\_GOB/MME\\_pt\\_Persist.html](http://iridl.ldeo.columbia.edu/maproom/Global/Drought/Global/CPC_GOB/MME_pt_Persist.html)

125 precipitation on various sectors and systems. It goes beyond assessing the mere accuracy of  
126 forecasted precipitation and aims to understand how well the forecasts translate into  
127 meaningful information for decision-making and risk management (AghaKouchak et al.,  
128 2023).

129  
130 Our main objective in this study is to evaluate the skill of the five state-of-the-art seasonal  
131 prediction systems from the Copernicus Climate Change Service (C3S) multi-model at a  
132 global scale in predicting particular features of extreme events which could lead to cascading  
133 hazards. These indices are defined by the Expert Team on Climate Change Detection and  
134 Indices (ETCCDI) and have been investigated in other studies (Chervenkov et al., 2019;  
135 Chervenkov & Slavov, 2019). These indices were designed to capture different aspects of  
136 precipitation such as timing and intensity and are useful in diagnosing the variability of  
137 precipitation at various timescales posing them as proper metrics for impact-based  
138 assessment. We refined these indices to capture weather patterns that could cause climate-  
139 induced hazards such as flood and wildfire. We conduct an evaluation of forecast models to  
140 assess their capability in discerning situations that result in the occurrence of a specific event  
141 from those that lead to its non-occurrence. As a related task, we perform a targeted analysis  
142 of model performance in regions with high risk of wildfires and floods. The following  
143 questions are answered in this study: Do seasonal forecast models have the capability to  
144 represent the variability of precipitation throughout the season? Is there a potential for  
145 combining various models to be an effective strategy for predicting extreme events,  
146 considering the variability of model performance across seasons and regions?

147

## 148 **2. Methodology**

149 This study examines the effectiveness of precipitation forecasts of five seasonal forecasting  
150 models from C3S project including the Centro Euro-Mediterraneo sui Cambiamenti Climatici  
151 (CMCC: version 35), Deutscher Wetterdienst (DWD: version 21), Environment and Climate  
152 Change Canada (ECCC: version 3), Météo France (Météo-France: version 8), and UK Met  
153 Office (UK-Met: version 601) models in accurately predicting extreme precipitation indices  
154 during the hindcast period spanning 1993 to 2016 (refer to Table S1). Validation was carried  
155 out using the fifth generation ECMWF reanalysis (ERA5) precipitation product.

156

### 157 **2.1 Data Preparation**

158 For our evaluation, we employed eight distinct climate extreme indices, following Expert  
159 Team on Climate Change Detection and Indices (ETCDDI)<sup>5</sup> definitions, to encompass  
160 different aspects of precipitation extremes, such as event duration, intensity, and frequency.  
161 We used 1mm, 10mm, and 20mm precipitation thresholds (representing wet days, heavy  
162 precipitation days, and very heavy precipitation days, respectively) for the calculation of  
163 climate extreme indices. We also used 75<sup>th</sup> and 95<sup>th</sup> percentiles of each grid in the reference  
164 datasets as a secondary constraint in calculating indices to be more representative of the local  
165 environmental conditions. Combination of metrics and thresholds resulted in generating a

---

<sup>5</sup> <https://www.wcrp-climate.org/data-etccdi>

166 comprehensive set of 28 climate extreme indices (refer to Table 1). These indices were  
 167 specifically designed to offer insights into the potential changes observed in precipitation  
 168 extremes over time and their impacts on various aspects of Earth system processes (Dunn et  
 169 al., 2022). The assessment of seasonal skill for the models was carried out using forecast  
 170 initializations on the first day of February, May, August, and November with a 1-month lead  
 171 time (i.e., March-May (MAM), June-August (JJA), September-November (SON), and  
 172 December-February (DJF) seasons respectively).

173

174 Table 1. List of climate extreme indices extracted and used to conduct this study.

abbreviation	Index	abbreviation	Index
cdd1	maximum consecutive dry days 1mm	nwd20q95	number of wet days 20mm and 95th percentile
cdd10	maximum consecutive dry days 10mm	fr1q75	fraction of precipitation over 1mm and 75th percentile
cdd20	maximum consecutive dry days 20mm	fr1q95	fraction of precipitation over 1mm and 95th percentile
cwd1	maximum consecutive wet days 1mm	fr10q75	fraction of precipitation over 10mm and 75th percentile
cwd10	maximum consecutive wet days 10mm	fr10q95	fraction of precipitation over 10mm and 95th percentile
cwd20	maximum consecutive wet days 20mm	fr20q75	fraction of precipitation over 20mm and 75th percentile
int1	daily pr intensity 1mm	fr20q95	fraction of precipitation over 20mm and 95th percentile
int10	daily pr intensity 10mm	hpd	Heavy precipitation days
int20	daily pr intensity 20mm	vhpd	very Heavy precipitation days
nwd1q75	number of wet days 1mm and 75th percentile	h1dp	Highest 1-day precipitation amount
nwd1q95	number of wet days 1mm and 95th percentile	h5dp	Highest 5-day precipitation amount
nwd10q75	number of wet days 10mm and 75th percentile	propd1	Proportion of days with precipitation at or above 1mm
nwd10q95	number of wet days 10mm and 95th percentile	propd10	Proportion of days with precipitation at or above 10mm
nwd20q75	number of wet days 20mm and 75th percentile	propd20	Proportion of days with precipitation at or above 20mm

175

176

177 The analysis was conducted on the ensemble mean for each model. All forecast models and  
 178 reference data were re-gridded to a consistent one-degree resolution. For spatial aggregation,  
 179 we conducted our analysis over the Intergovernmental Panel on Climate Change (IPCC)  
 180 regions shown in Table S2 (Iturbide et al., 2020). The IPCC divides the world into major  
 181 regions, each of which includes a group of countries or territories that share similar climate  
 182 characteristics, geographic features, and socio-economic factors. The IPCC regions, also  
 183 known as the "IPCC Regional Reporting", are a set of geographical regions used by the IPCC  
 184 as a framework for understanding how climate change affects different parts of the world and  
 185 to facilitate the assessment of climate change impact, vulnerability, and adaptation strategies  
 186 at the regional level.

187

## 188 2.2 Model Evaluation

189 For evaluation and comparison of forecast models against reference data, we employed  
 190 percentage bias with an optimal value of zero. Here, zero signifies a perfect alignment  
 191 between model predictions and observed data, and positive-bias/negative-bias signifies over-  
 192 estimation/under-estimation (Eq.1).

193

$$PBIAS = 100 \frac{\sum_{i=1}^N (S_i - O_i)}{\sum_{i=1}^N O_i} \quad \text{Eq.1}$$

194

195 where  $S_i$  is the model simulation and  $O_i$  is the observed value at time  $i$ .

196

197 We also conducted a discriminant analysis to determine if the forecast skill varied in different  
 198 sections of the precipitation distribution. To achieve this, we categorized the outcomes into

199 three distinct groups using upper and lower terciles: one-third representing below-normal  
200 conditions (lower tercile), another third representing above-normal conditions (upper tercile),  
201 and the remaining third representing conditions falling between the lower and upper tercile.  
202 Utilizing a random forest classification, we conducted a classification based on 75 percent of  
203 the available datasets (training sets). Subsequently, we computed the area under the ROC  
204 curve which is often used as a summary measure of forecast discrimination for the test data.  
205 ROC score is an efficient way to analyze the overall discriminatory power of the forecasts. It  
206 takes values between 0 to 1. Here we categorized the ROC score to level of discrimination  
207 (i.e., in our case ability to discriminate extreme events from non-extreme events). The values  
208 of ROC score between 0.0 to 0.6 is considered no discrimination, 0.6 to 0.7 is considered  
209 satisfactory discrimination, 0.7 to 0.8 is considered good discrimination, 0.8 to 0.9 is  
210 considered very good discrimination, and 0.9 to 1.0 is considered excellent discrimination  
211 (Mandrekar, 2010). Also, we conducted Kendall's Tau rank correlation analysis to measure  
212 the strength of the relationship between climatic indices extracted from forecast models and  
213 reference data aggregated over each IPCC regions (Sen, 1968). These metrics were utilized to  
214 assess the skill of the forecast models in capturing extreme events and their associated  
215 accuracy.

216

### 217 **2.3 Impact based framework**

218 The IPCC regions which were vulnerable to wildfire and flooding were identified by  
219 categorizing them based on the proportion of farmland (Friedl & Sulla-Menashe, 2022),  
220 proportion of burned areas (Chuvieco et al., 2018; Lizundia-Loiola et al., 2020), percentage  
221 of flood-affected zones (Tellman et al., 2021), proportion of built-up regions (Gong et al.,  
222 2020), and population density (Schiavina et al., 2023) (see Figure S1). We specifically  
223 focused on regions that not only had an elevated risk of wildfire (flood) exposure, but also  
224 had a significant built-up area and population density (substantial agricultural presence and  
225 population density). These selected regions were earmarked for additional analysis.

226

227 We carefully selected relevant extreme indices pertinent to the corresponding climate-  
228 induced hazard in each region. For the regions with wildfire as a prominent natural hazard we  
229 selected maximum consecutive dry days 1mm (cdd1), and proportion of days with  
230 precipitation at or above 1mm (propd1) indices as the relevant indicators of a weather  
231 condition conducive to wildfire. For regions with a high risk of flooding, we selected number  
232 of wet days with 10mm precipitation and 75th percentile of the reference data (nwd10q75)  
233 and heavy precipitation days (hpd) indices as the relevant indicators. We also determined the  
234 season with the highest occurrence rate for each specific hazard and regions. In every region,  
235 we identified the top-performing model in terms of predictive accuracy using the following  
236 selection criteria. Initially, we prioritized models with a combination of higher correlation  
237 (statistically significant) and lower bias. If multiple models demonstrated similar high  
238 performance compared to the others, we utilized a Taylor diagram to select models that  
239 aligned more closely with the reference data across various performance metrics. Our  
240 evaluation then focused on assessing the models' forecast skill with respect to relevant  
241 indices in the identified hazard-prone seasons for each region. By adopting this impact-based

242 approach, we aimed to pinpoint the most suitable models and indices for each climate-  
243 induced hazard, enabling more effective and tailored climate risk assessments.

244  
245  
246

### 247 **3. Results**

#### 248 **3.1 Global Analysis of Model Bias**

249 The analysis of percentage bias at a global scale across the four seasons reveals a consistent  
250 tendency of underestimation in all forecast models with respect to reference data for most of  
251 the extreme wet and extreme dry precipitation indices (Figure 1 shows UK-Met model as an  
252 example, and Figures S2-S5 show other models). The cdd1 index, which measures the  
253 maximum consecutive dry days at 1mm threshold, shows negative bias for most but not all  
254 regions, implying that the models predict a lower number of dry days than observed. In the  
255 case of the cwd1 and propd1 indices, which measures the maximum consecutive wet days at  
256 1mm threshold and proportion of days with at least 1mm precipitation, all models exhibit a  
257 positive bias, suggesting that they predict a higher number of wet days than observed data.

258

259 For wet indices, all models underestimate cwd10 and cwd20 indices (10- and 20-mm  
260 precipitation threshold, respectively) across the four seasons and most of the IPCC regions.  
261 The models exhibit lower bias for extreme indices that are defined based on a 10mm  
262 precipitation threshold. As the threshold increases, so does the bias. This pattern is consistent  
263 with the findings of regional C3S assessment studies, for example in Africa (Gebrechorkos et  
264 al., 2022). These observations underscore the limitations in forecast capabilities for  
265 accurately modelling persistent wet and dry periods. By introducing secondary constraints  
266 (i.e., 75th, and 95th percentiles of the reference data) to the indices, the bias increases  
267 signifying the models' limitation in capturing more severe extreme events.

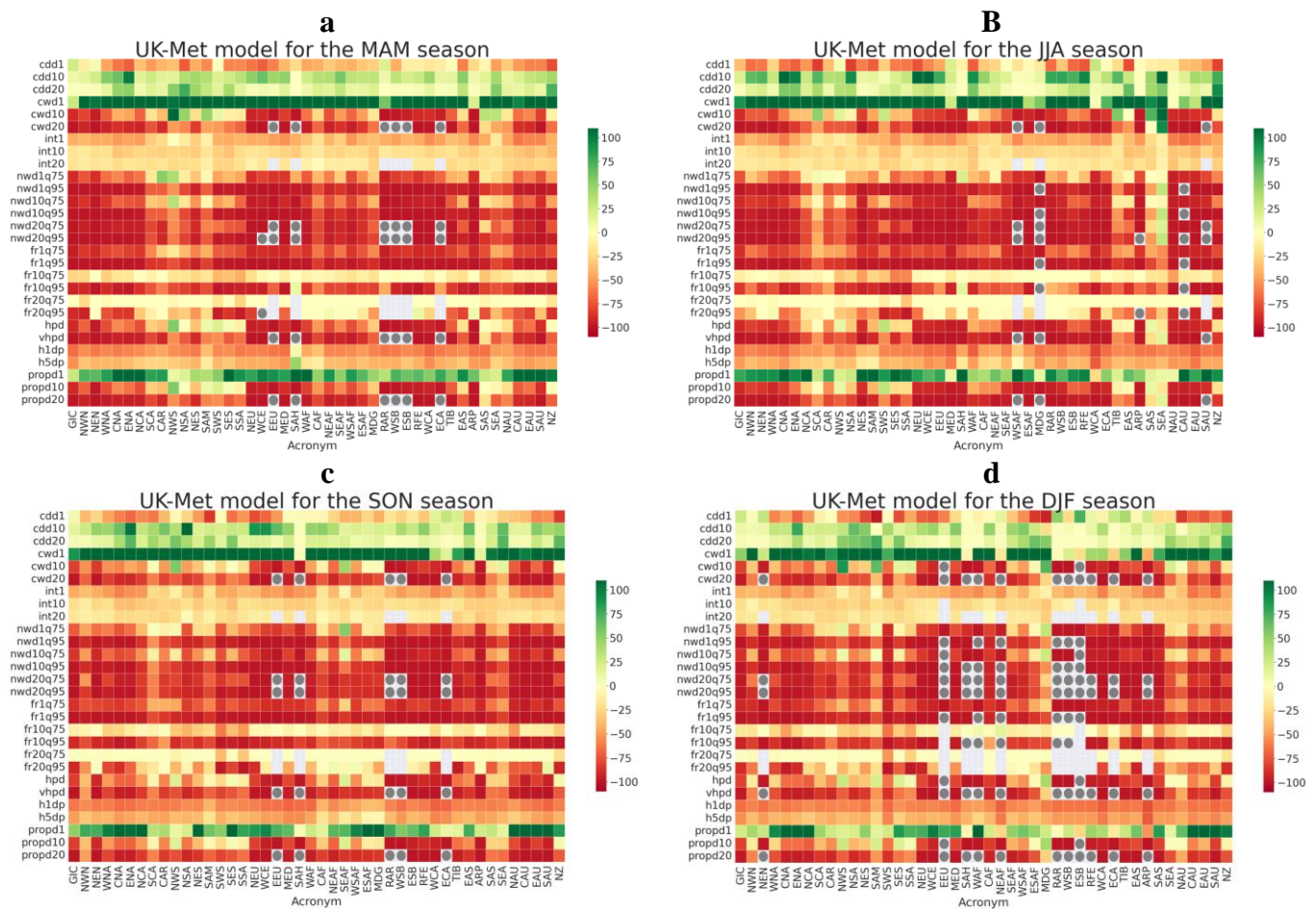
268

269 Figure 1 and Figures S2-S5 show that the CMCC, DWD, and ECCC models demonstrate  
270 relatively lower ability to capture extreme rainfall events within the extratropical IPCC  
271 regions compared to the UK-Met and Météo-France models, particularly when 95<sup>th</sup>  
272 percentiles of the reference dataset are introduced as thresholds to the index. This observation  
273 is consistent across all four seasons. However, in the tropical and subtropical regions, all  
274 models (especially UK-Met and Météo-France models) exhibit relatively better performance  
275 (lower bias) in capturing extreme events, compared to extratropical regions, when 75<sup>th</sup> and  
276 95<sup>th</sup> percentile thresholds were used in the indices as additional constraints. This is attributed  
277 to the model's predictive skill in grasping large-scale teleconnection patterns (Giuntoli et al.,  
278 2022).

279

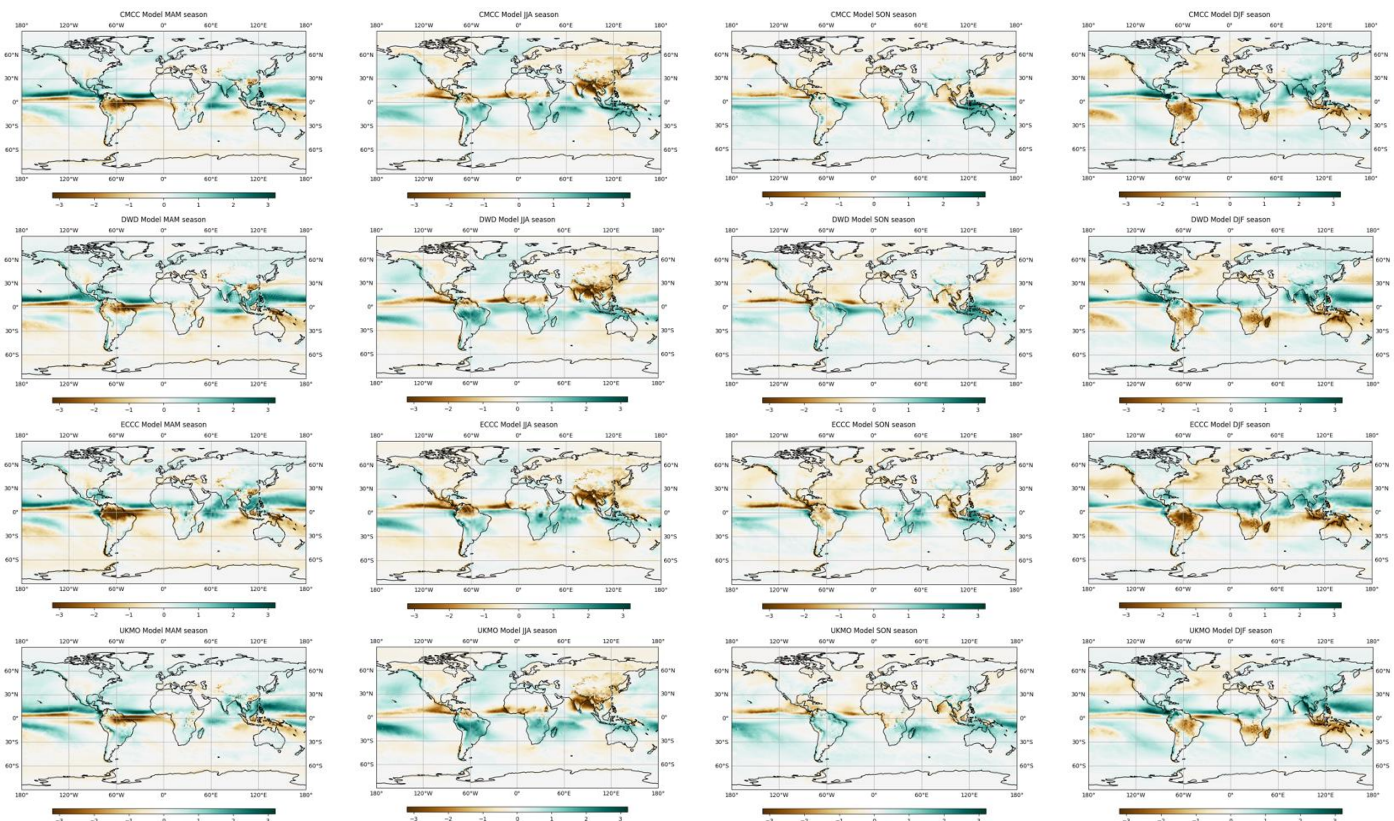
280 Figure 2 shows the standardized precipitation anomalies of the five models across the four  
281 seasons. Standardized anomalies offer invaluable insights about the localized anomalies  
282 through the number of standard deviation departure of forecasts from observations. We  
283 normalized the precipitation anomalies against the climatological standard deviation in each  
284 grid. A notable tendency to produce a double Intertropical Convergence Zone with significant  
285 anomalies over tropical pacific is observed in all models (García-Franco et al., 2023). The

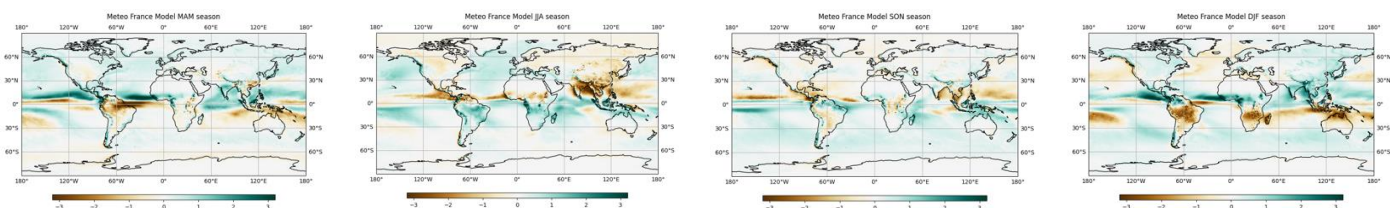
286 pattern of anomalies differs substantially across seasons for all model with MAM, JJA, and  
 287 DJF seasons showing larger anomalies in the tropical, subtropical, and equatorial regions,  
 288 while SON season show lower levels of anomaly. In the northern hemisphere's extratropical  
 289 land regions, seasonal forecasts reveal a larger negative anomaly in summer and larger  
 290 positive anomalies in winter compared to spring and autumn respectively, which is likely due  
 291 to the increased influence of local factors on summertime and wintertime precipitation.  
 292 Uncertainties in these forecasts are largely attributed to model parameterization, including  
 293 elements such as vegetation cover and cloud physics, which can significantly impact  
 294 precipitation predictions (Borovikov et al., 2019).  
 295



296 Figure 1. Percentage bias of UK-Met model for a) MAM, b) JJA, c) SON, and d) DJF  
 297 seasons. Grids indicated in gray circles shows the regions where reference data indicated the  
 298 existence of extreme events while the forecast models couldn't capture any events satisfying  
 299 the index requirements. Grids with no values reflect regions that both reference data and  
 300 forecasts did not capture any events satisfying the index requirements. The color bar is  
 301 limited to the range of -100 to 100 for visualization purposes. This range was chosen to  
 302 enhance visibility of variations in regions with small bias, which is of particular significance  
 303 in this context. It should be noted that the actual values occasionally exceed this range but  
 304 were truncated to facilitate better visual interpretation.  
 305  
 306

307 Overall, the precipitation anomalies are markedly larger in equatorial regions, and it  
 308 decreases toward the northern and southern extra-tropical regions. Conversely, when  
 309 assessing the percentage bias for climatic indices, we observe a higher bias in the extra-  
 310 tropical regions and a lower bias in equatorial regions. In the extra-tropical regions, forecast  
 311 models demonstrate a reasonable ability to predict total precipitation three months in advance  
 312 but face challenges when estimating seasonal precipitation patterns and variation throughout  
 313 the four seasons (for example estimating number of consecutive wet days/dry days).  
 314 Although, in equatorial regions, the elevated levels of precipitation contribute to a higher  
 315 anomaly in total precipitation, the models exhibit greater skill in predicting seasonal rainfall  
 316 patterns, and consequently climatic indices, with a three-month lead time. This is partially  
 317 attributable to more uniform precipitation patterns throughout the year in equatorial regions.  
 318 For indices measured in terms of the number of days, we observe larger bias compared to  
 319 those representing total rainfall, indicating the models' limited ability to accurately replicate  
 320 the variation of precipitation throughout the season (Figure 1). Indices that represent  
 321 magnitude and intensity of precipitation (i.e., precipitation intensity, fraction of precipitation,  
 322 highest 1-day precipitation amount, and highest 5-day precipitation amount) exhibit lower  
 323 biases, suggesting that the model's skill in simulating total seasonal precipitation. The UK-  
 324 Met and Météo-France models exhibit higher capacity in capturing extreme events,  
 325 demonstrating favorable performance across various regions when considering 75<sup>th</sup> and 95<sup>th</sup>  
 326 percentile threshold levels. Moreover, even for indices not explicitly based on local  
 327 thresholds, the biases for the UK-Met and Météo-France models remain lower compared to  
 328 other models across the globe.  
 329  
 330





331 Figure 2. Standardized precipitation anomalies for CMCC (row 1), DWD (row 2), ECCC  
 332 (row 3), UK-Met (row 4), and Météo-France (row 5) and during MAM (column 1), JJA  
 333 (column 2), SON (column 3), and DJF (column 4). Anomalies are shown in terms of number  
 334 of standard deviation departure of forecasts from observations in each grid.

335

### 336 3.2 Global Analysis of ROC Scores

337

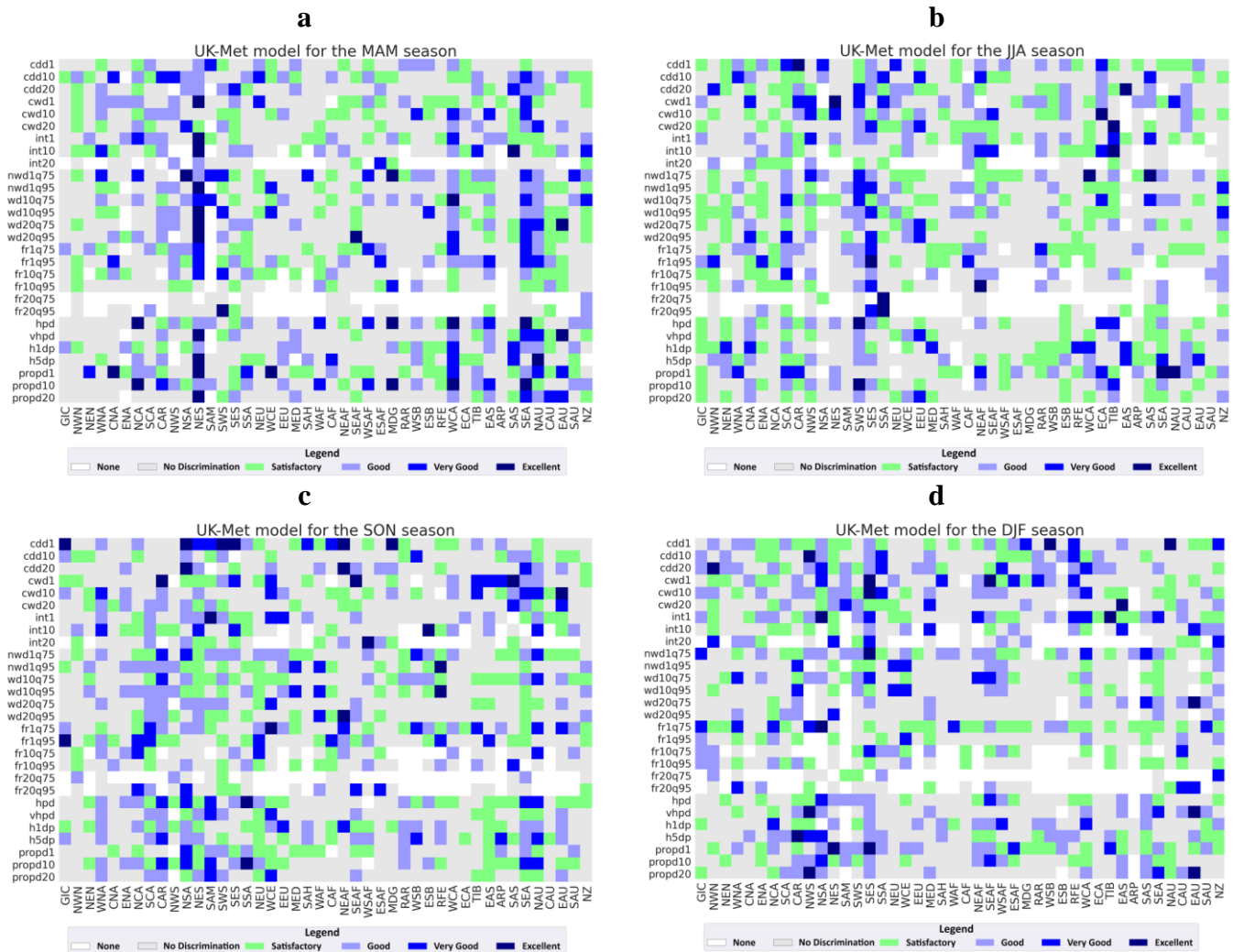
338 While bias analysis assesses the systematic errors that exist in the forecasts, discrimination  
 339 analysis is a useful to measure on how well the year-to-year variations in the forecasted  
 340 values match those in the observations. Measurements of ROC score in Figure 3 and Figures  
 341 S6-S9 show higher performance of forecast models in the intertropical regions located in  
 342 Atlantic, Indian ocean, and west Pacific regions (Guimarães et al., 2021; Jie et al., 2017). The  
 343 skill level varies across different models and seasons across Africa (refer to Table S2 for the  
 344 complete names of IPCC regions). Notably, the Météo-France and UK-Met models exhibit  
 345 superior performance during the SON and DJF seasons (i.e., indices with satisfactory, good,  
 346 very good, and excellent discriminations are more frequent for these models). The  
 347 exceptional performance of the Météo-France model in African regions has been the subject  
 348 of discussion in prior studies (Gebrechorkos et al., 2022). Furthermore, when considering the  
 349 ROC scores, the UK-Met model demonstrates a higher level of skill compared to the other  
 350 four models in predicting extreme events in several Australian regions. This elevated skill of  
 351 the UK-Met model is particularly pronounced during the MAM season whereas in JJA, SON,  
 352 and DJF the skill drops dramatically. The lower performance of ACCESS-S1 forecast model  
 353 (which is the same model used in UK-Met but with different ensemble generation scheme,  
 354 ensemble size and the configuration of the system for operational forecasting) over Australia  
 355 during southern hemisphere summer (DJF) is also concluded in other studies (King et al.,  
 356 2020).

357

358 The prevalence of grids with no discrimination ROC categories is more pronounced in  
 359 extratropical regions, possibly due to the inherent unpredictability of extratropical variations  
 360 and limitations within the models when it comes to representing interactions between tropical  
 361 and extratropical regions, as well as land surface processes (De Andrade et al., 2019).  
 362 Notably, the CMCC, DWD, and ECCC models are associated with many regions where the  
 363 models fail to detect any extreme event, as indicated by the absence of discrimination  
 364 categories in Figures S6-S8. This disparity in extratropical regions is particularly conspicuous  
 365 when compared to the UK-Met and Météo-France models. Specifically, the divergence is  
 366 most apparent for wet day indices corresponding to the 75th and 95th percentiles of the  
 367 reference data. This suggests that the CMCC, DWD, and ECCC models encounter challenges  
 368 in accurately simulating extreme precipitation events exceeding the 75th and 95th percentiles  
 369 of the reference dataset across a larger portion of the IPCC regions.

370  
 371  
 372  
 373  
 374  
 375  
 376  
 377  
 378

In certain tropical regions, there is a notably higher occurrence of indices falling within at least the satisfactory discrimination category when compared to other regions across all five models. Based on bias and ROC score analysis, the skill of C3S models vary markedly across regions. Hence, it is imperative to establish an impact-based framework for targeted selection of models tailored to address specific climate-related hazards in each region. This approach is crucial in ensuring effective and accurate responses to extreme weather events.



379 Figure 3. Discrimination levels using categorized ROC score for UK-Met model for a)  
 380 MAM, b) JJA, c) SON, and d) DJF seasons. Grids that are shaded in white represent regions  
 381 that either or both reference data and model did not capture any events satisfying the index  
 382 requirements.

### 3.3 Global Analysis of Wildfire-related Indices

385 Many scientific investigations have underscored the notable influence of climatic patterns on  
 386 the initiation of wildfires (Sharma et al., 2022; Turco et al., 2023). Extended periods  
 387 characterized by elevated temperatures devoid of precipitation events establish an  
 388 environment conducive to fire ignition and propagation, intensifying the combustibility of  
 389

390 vegetative layers (Alizadeh et al., 2021, 2023). As the duration of consecutive dry days (days  
391 without rainfall or with rainfall below a specific threshold) extends, the moisture content of  
392 fuel diminishes, increasing its susceptibility to ignition (Abatzoglou & Williams, 2016). In  
393 this section, we investigate the cdd1 and propd1 indices to assess the predictive skill of  
394 models on a global scale and then within the IPCC region, where wildfires emerge a  
395 prominent natural hazard.

396

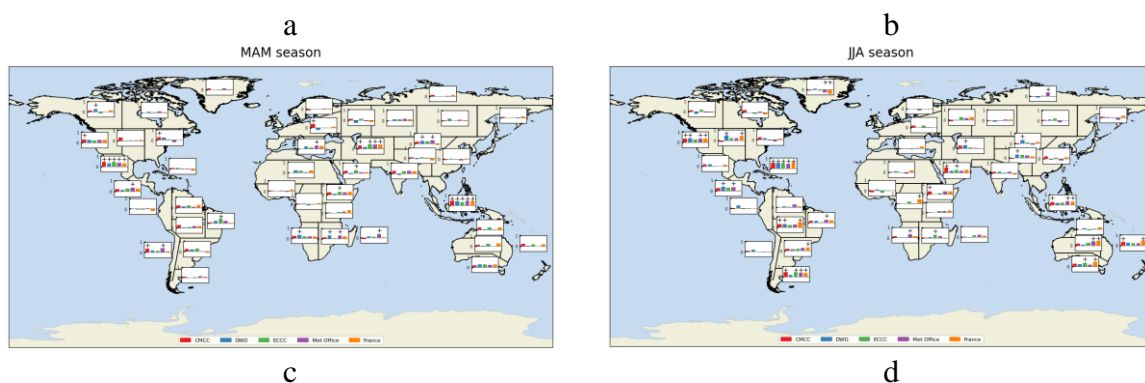
397 The evaluation results reveal that the performance of the models varies across different  
398 regions. This regional variation highlights the unique strengths and adaptability of each  
399 model, as they excel in response to the specific challenges and requirements posed by distinct  
400 geographic areas. The examination of global Kendall's Tau correlation scores based on the  
401 cdd1 index reveals that the models' predictive abilities are most pronounced in the  
402 intertropical and subtropical zones (Figure 4). While model performance varies notably  
403 across different seasons, at least one model displays a notable correlation with the reference  
404 datasets within each season and region. Same rule applies to the IPCC regions located in  
405 southern parts of Africa and Oceania continents. The predictive skill of the models is also  
406 pronounced in the West Central Asia (WCA), East Central Asia (ECA), Tibetan Plateau  
407 (TIB), and regions located in Australia and southern America.

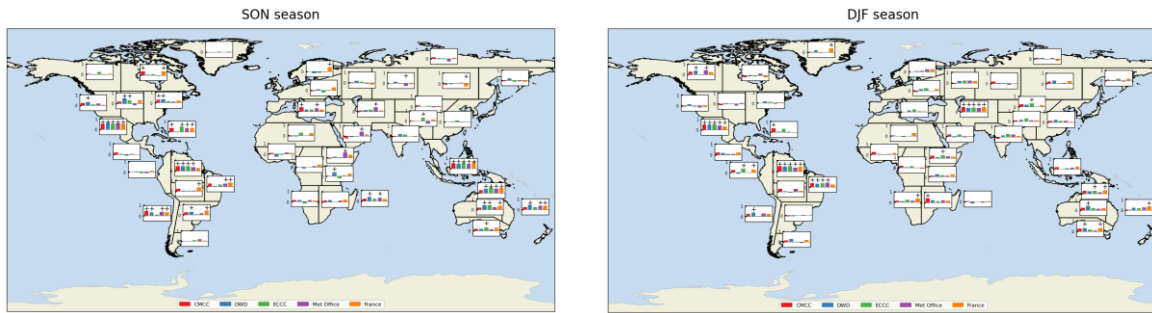
408

409 Percentage bias results show that most of the models generally underestimate cdd1 across all  
410 seasons except for northern regions near the pole during the MAM and DJF seasons which  
411 show overestimation (Figure 5). The considerable bias in the southern hemisphere during the  
412 DJF season is particularly noteworthy, which can be linked to the shortfall in predictive  
413 accuracy of the forecast models in extratropical areas. In contrast, the reduced bias levels, and  
414 the significant correlation of models and observations such as south and southeast Asia,  
415 particularly during dry seasons, can be attributed to the influence of soil moisture memory on  
416 the predictive capabilities of the forecast models in this region (Zhou et al., 2021).

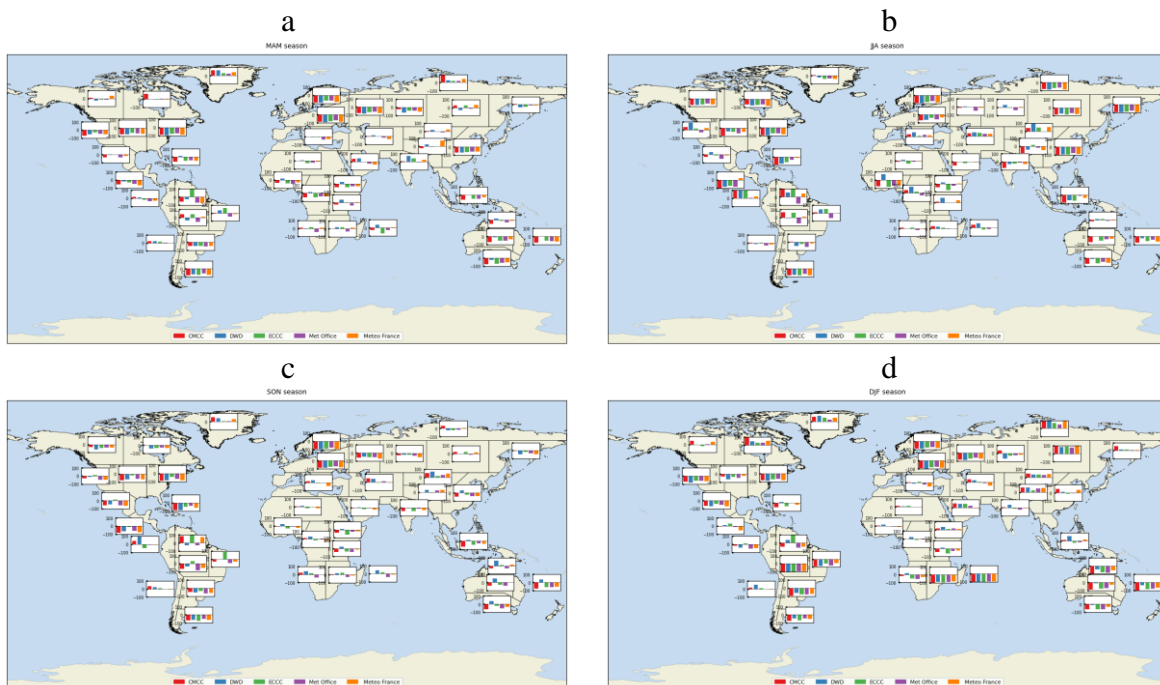
417

418





419 Figure 4. Kendall's Tau coefficients for the cdd1 index in IPCC regions during a) MAM, b)  
 420 JJA, c) SON, and d) DJF. Models with a significant correlation coefficient at the 0.05 level  
 421 are marked with a plus sign.  
 422  
 423  
 424  
 425  
 426



427 Figure 5. Percent bias for cdd1 index in IPCC regions during a) MAM, b) JJA, c) SON, and  
 428 d) DJF.  
 429  
 430

431 In the southern hemisphere, and in the JJA, SON, and DJF seasons, the correlation coefficient  
 432 for almost all models on the propd1 index is highly significant, apart from southern Africa  
 433 where the models show notable skill only in the DJF season (refer to Figure S10). Notably,  
 434 the bias values for these southern hemisphere regions are both positive and large. This  
 435 indicates that while the models can accurately represent the seasonal variations, they  
 436 consistently overestimate the duration of wet days throughout the seasons (refer to Figure  
 437 S13). In North American regions, the correlation coefficient of models fluctuates seasonally,  
 438 with noteworthy performance during the JJA and SON seasons. In contrast, for areas across  
 439 Asia, the models perform significantly well only in the winter season (i.e., DJF). All Models

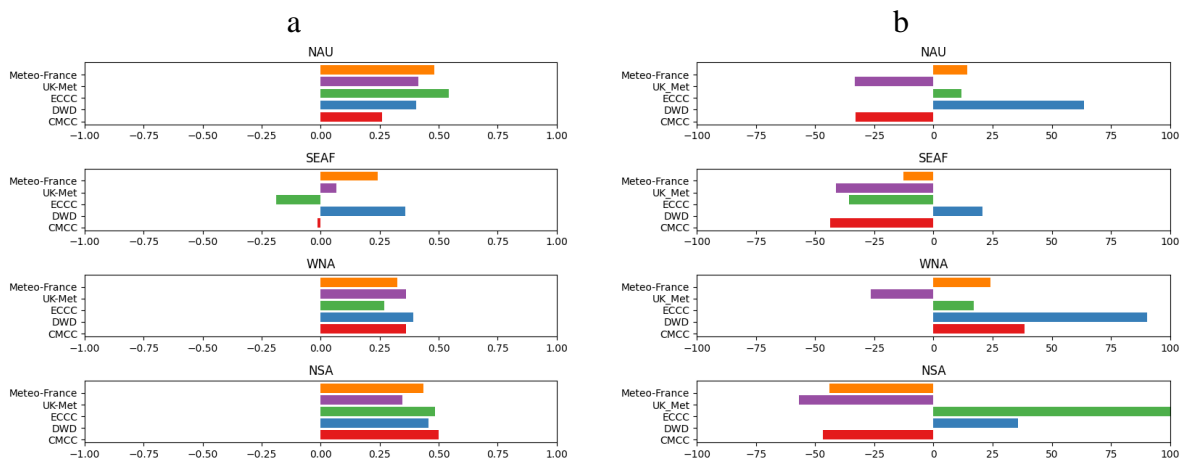
440 demonstrate strong predictive power throughout all seasons in the WCA region. It's important  
 441 to note that although the bias is generally large and positive in most northern hemisphere  
 442 regions, the bias is significantly lower in Asian regions during the DJF season compared to  
 443 North America and Europe (refer to Figure S10-S11).  
 444

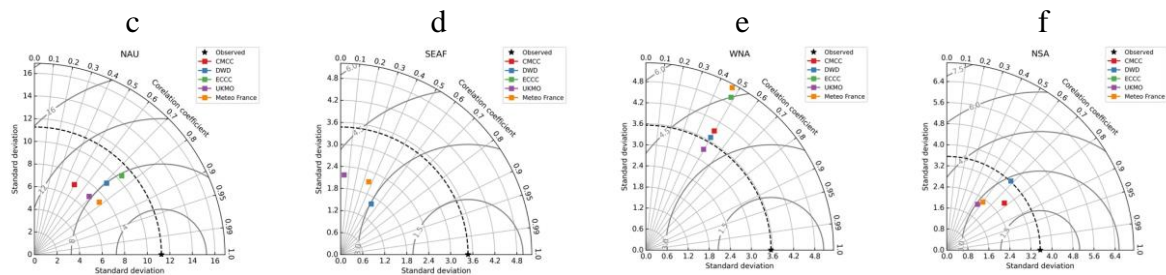
### 445 3.4 Wildfire-prone Regions: Targeted Forecast Performance Analysis

446 We now focus on the four regions where the wildfire is a prominent natural hazard: NAU,  
 447 SEAF, Western North America (WNA), and NSA regions. Within each region, a particular  
 448 season characterized by an elevated likelihood of wildfire incidence has been designated for  
 449 subsequent analysis and processing.  
 450

451 In northern Australia, the peak period for wildfire aligns with the dry SON season. From  
 452 August to December, many regions of Southern Africa experience the onset of their wildfire  
 453 season therefore we selected the SON season for further analysis. In the United States,  
 454 wildfire activity is a year-round concern, but the most severe wildfires arise during the  
 455 summer months (JJA season), particularly in the western regions. In Latin America, the fire  
 456 season typically commences at the end of January and extends through April (DJF season).  
 457

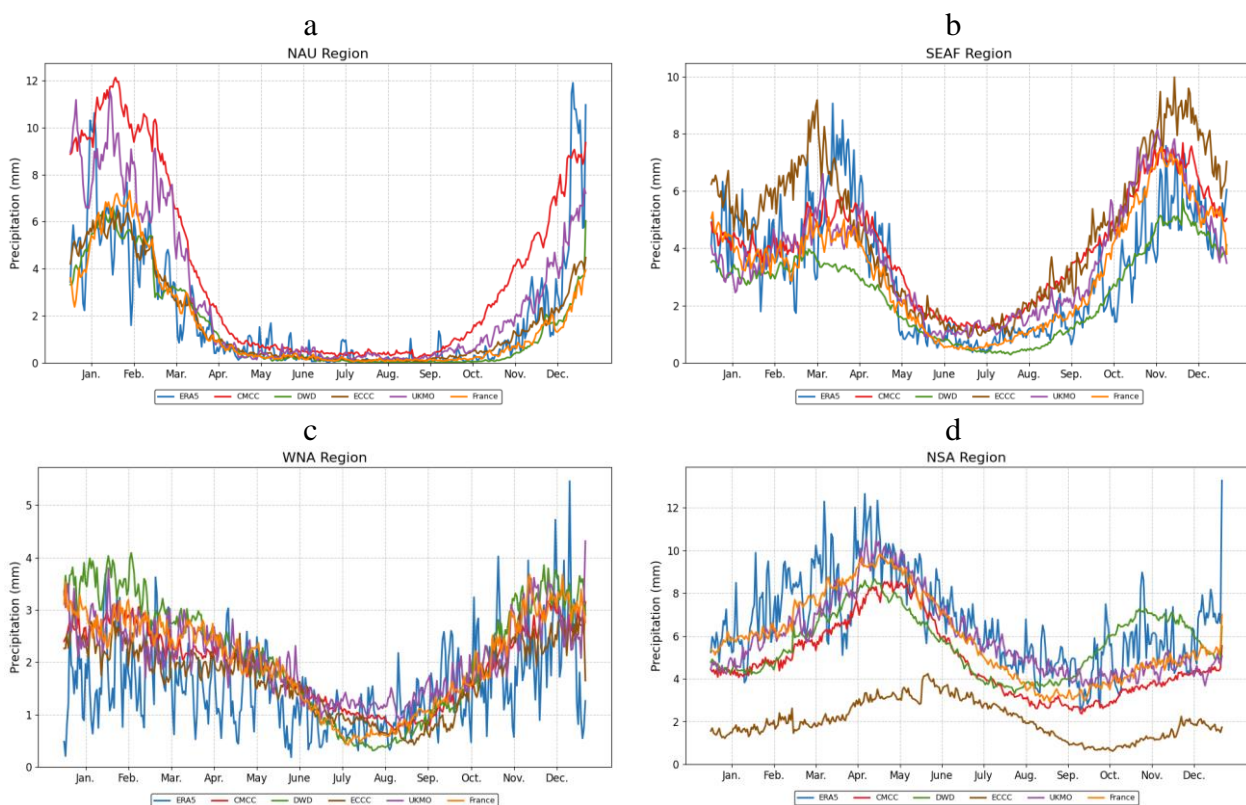
458 In Figure 6a, it is evident that all models except for CMCC demonstrate a notable correlation  
 459 with the reference data for the maximum number of consecutive dry days in the NAU region.  
 460 Notably, Météo-France and ECCC models exhibit the strongest correlation, positioning them  
 461 as prominent contenders. Furthermore, in Figure 6b both Météo-France and ECCC display  
 462 lower bias, demonstrating their predictive potential. However, in the Taylor diagram  
 463 presented in Figure 6c, the ECCC model establishes its supremacy over Météo-France by  
 464 exhibiting a standard deviation that is more closely aligned with the reference data. The  
 465 overestimation of precipitation (and consequently underestimation of dry days) in CMCC and  
 466 UK-Met models over NAU region is visible in Figure 7 where they exceed the 1mm  
 467 threshold earlier and with steeper slope compared to other models resulting in the  
 468 underestimation of cdd1 index.  
 469  
 470  
 471





472 Figure 6. Performance metrics for the maximum consecutive dry days index with 1mm  
 473 precipitation threshold (cdd1): a) Kendall's Tau coefficient, b) Percentage bias, and Taylor  
 474 diagram for c) NAU, d) SEAF, e) WNA, and f) NSA regions respectively.

475  
 476  
 477  
 478  
 479  
 480  
 481  
 482



483 Figure 7. Annual climatology time series of the precipitation for five C3S models and the  
 484 ERA5 datasets over NAU, SEAF, WNA, and NSA region.

485  
 486

487 This model selection framework is extended for other three region and the main findings  
 488 reveal distinct model performance variations in different regions. The ECCC model is  
 489 particularly strong in forecasting consecutive dry days in the NAU region and closely tracks  
 490 reference data. In contrast, the DWD model emerges as the top performer in the SEAF and

491 NSA regions, exhibiting the highest correlation, lower bias, and lower root mean square error  
492 in these areas. The UK-Met model excels in the WNA region, demonstrating a close match  
493 with the reference dataset's standard deviation. These variations in model performance are  
494 attributed to their abilities to simulate significant large-scale climate variabilities such as  
495 ENSO, IOD, and north Australian SSTs, which play a crucial role in enhancing prediction  
496 skill during the SON season over Australia.

497

498 In the domain of predicting the proportion of wet days featuring precipitation exceeding 1mm  
499 (propd1), the Météo-France model exhibits superior overall performance in the NAU region,  
500 with high correlation values. Additionally, Météo-France demonstrates notably lower bias  
501 values, as shown in Figure S12a and S12b. Although Figure S12c's Taylor diagram reveals  
502 that Météo-France has a standard deviation that is slightly worse than other models, the bias  
503 metric indicates the superiority of the Météo-France model. In the SEAF region Météo-  
504 France and DWD model exhibit superior overall performance over other models according to  
505 correlation and bias values in Figure S12 and S12b. Based on the Taylor diagram, Météo-  
506 France has a standard deviation closer to the reference data. The substantial correlation  
507 difference and standard deviation indicates the superiority of Météo-France model. The  
508 overestimation of the propd1 index in Météo-France model compared to DWD model can be  
509 concluded from Figure 7b where the time series of precipitation of Météo-France is  
510 overestimating that of reference datasets during SON season.

511

512 For the WNA region, the ECCC model exhibits a higher correlation score but notably high  
513 bias values. The absence of substantial correlation values in other models results in the choice  
514 of the ECCC model as the most favorable option. In the NSA region, it's evident that the  
515 DWD model stands out as the top-performing model. It boasts a high correlation score, the  
516 smallest bias when compared to other models, and a standard deviation that closely aligns  
517 with the reference data (Figure S12a and S12b and S12f).

518

### 519 **3.5 Global Analysis of Flood-related Indices**

520 Consecutive occurrences of extreme precipitation over successive days can significantly  
521 elevate the probability of widespread flooding. Many investigations have documented  
522 instances of substantial flooding due to consecutive multi-day extreme precipitation incidents  
523 (Ávila et al., 2016; Du et al., 2022; Rivoire et al., 2023). To assess the capabilities of the C3S  
524 models across IPCC regions, where flooding is a predominant natural hazard, we employed  
525 the heavy precipitation days index (hpd) and number of wet days with 10mm precipitation  
526 threshold index exceeding the 75th percentiles of the reference dataset (nwd10q75).

527

528 According to Figure S13, the correlation of all models with the reference data, as assessed by  
529 the hpd index, is most evident in Central and South America, particularly during the JJA and  
530 SON seasons. Also, regions in central Africa shows noticeable predictive abilities in the DJF  
531 season over CMCC, and Météo-France, and for regions in Australia the CMCC model  
532 demonstrate noticeable results throughout the year, excluding the winter season (JJA).  
533 Percent bias values are large and negative for all models and across all seasons in northern  
534 hemisphere extratropical regions suggesting the inadequacy of models in capturing heavy

535 precipitation days in these areas. In the tropical and sub-tropical regions bias values are  
536 markedly smaller especially during MAM, JJA and SON seasons. For the regions located in  
537 Australia across all seasons the model bias is large and negative. While the bias for north  
538 African regions is relatively smaller in DJF season, for other seasons the bias values are large  
539 and negative. The bias values in south American regions in extratropic is relatively lower  
540 than those of Africa and Australia across MAM, and DJF the seasons.

541

542 In Central and Northern Europe, ECCC, and DWD models show significant predictive  
543 abilities during the winter season (DJF). For Europe, the predictive skill of models for  
544 extreme precipitation events is higher in DJF; for the other seasons, predictive skill is poor as  
545 reported in other studies (Rivoire et al., 2023). The models are generally weak in their  
546 predictions for IPCC regions in Asia, apart from the southern and southeastern areas,  
547 including WCA, TIB, SAS, and East Asia, where CMCC, UK-Met and Météo-France models  
548 exhibit noteworthy predictive skill except for the JJA season. In North America, the models'  
549 predictive capacities are lacking across all seasons. Meanwhile, there is a noticeable negative  
550 bias in the predictive skill of all models, especially in extratropical regions of both the  
551 Southern and Northern Hemispheres as shown in Figure S14. These biases are comparatively  
552 smaller in the Western Pacific and Atlantic equatorial regions.

553

554 Regarding the nwd10q75 index, its characteristics mirror those of the hpd index, apart from  
555 the 75th percentile constraint in the reference data (as seen in Figures S15 and S16). In  
556 essence, the patterns of different models across various seasons and regions are nearly  
557 identical to those observed for the hpd index. Models that have some, albeit weak, predictive  
558 abilities based on the hpd index generally lose their predictive strength when evaluated using  
559 the nwd10q75 index.

560

### 561 **3.6 Flood-prone Regions: Targeted Forecast Performance Analysis**

562 In the South-East Asia (SEA) monsoon region during JJA (flood season), the UK-Met  
563 demonstrates a superior performance compared to other models, exhibiting notably high  
564 correlation and lower bias values (Figure 8.a and 8b). Although, the Taylor diagram indicates  
565 that UK-Met exhibits a larger standard deviation value compared to other models but the  
566 markedly lower bias values make this model the optimal choice here (Figure 8c). This is also  
567 evident in the Figure 9a where Météo-France shows overestimation of precipitation, ECCC  
568 shows underestimation, while UK-Met, DWD, and CMCC follow the reference precipitation  
569 very closely. Overall, in this region the prediction skill is mostly highlighted in the pre-  
570 monsoon (April–May) and post-monsoon (October–November), while during monsoon  
571 seasons (JJA) skill is poorer because of the monsoon influences on precipitation predictability  
572 (Wanthanaporn et al., 2023).

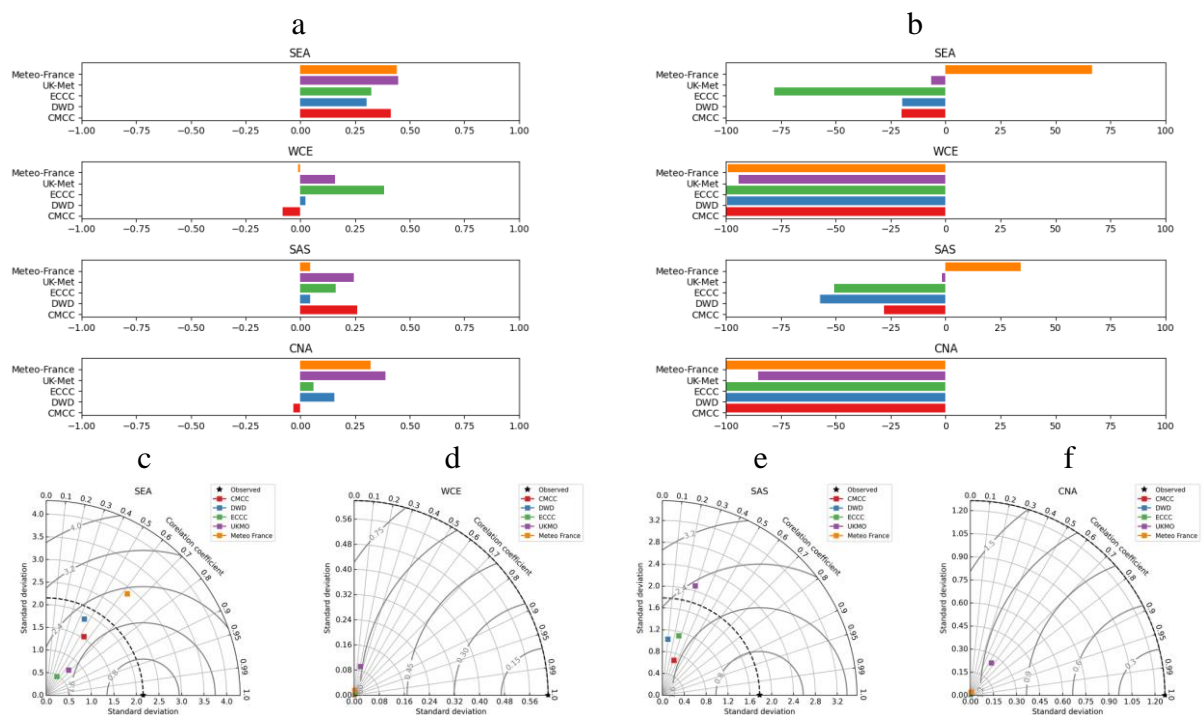
573

574 Based on Figure 8, in the Western and Central Europe (WCE) region during the DJF flooding  
575 season, the ECCC model exhibits higher significant correlation values compared to other  
576 models. However, all models struggle to adequately capture reference data variations, as  
577 indicated by high RMSE values and low correlation coefficients. In the South Asia (SAS)  
578 region during the JJA season, the UK-Met and CMCC models demonstrate higher correlation

579 values, with the UK-Met model showing positive but statistically insignificant correlation.  
 580 The UK-Met model outperforms others by exhibiting smaller bias, particularly in comparison  
 581 to the CMCC model. Therefore, the UK-Met model is favored for the SAS region. In the  
 582 Central North America (CNA) region during the JJA season, both the UK-Met and Météo-  
 583 France models exhibit significant correlation coefficients, while all models display large bias  
 584 values. Once again, the UK-Met model stands out due to its lower bias compared to the other  
 585 models.

586  
 587 Upon eliminating the constraint associated with the 75th percentile of the reference data in  
 588 predicting heavy precipitation days, there is an observable reduction in bias values across  
 589 SEA and SAS regions for the hpd index (Figure S17 and S17b). The correlation values are  
 590 almost like those of nwd10q75 index. Simultaneously, the standard deviation values become  
 591 more aligned with the reference data (Figure S17c and S17f). However, it is important to note  
 592 that despite these changes, the hierarchy of model selection remains consistent. This  
 593 highlights that the models are relatively less effective at capturing anomalies linked to an  
 594 increase in the impact of local factors.

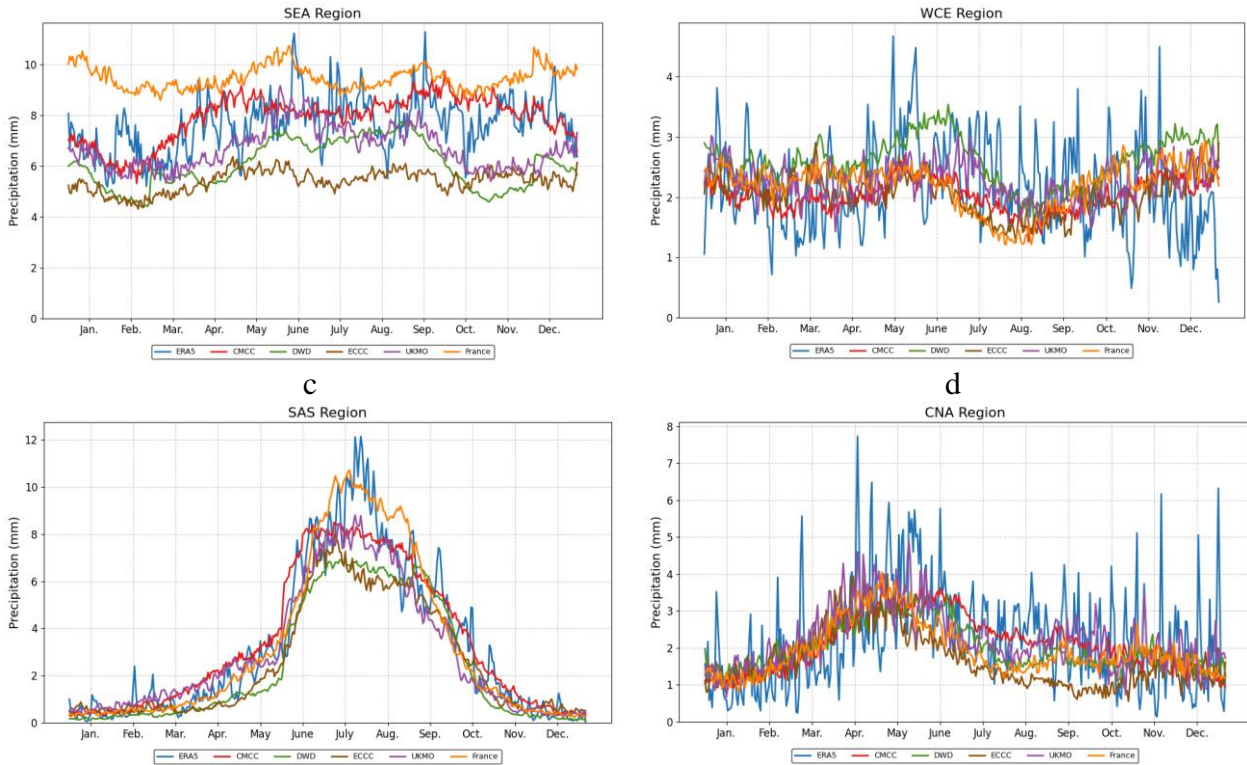
595  
 596  
 597



598 Figure 8. Model performance with respect to the number of heavy precipitation days  
 599 exceeding 10 mm and the 75th percentiles of the reference dataset (nwd10q75): a) Kendall's  
 600 Tau coefficient, b) Percentage bias, and Taylor diagram for c) SEA, d) WCE, e) SAS, and f)  
 601 CNA regions, respectively.

a

b



602 Figure 9. Annual climatology time series of the precipitation for five C3S the ERA5 datasets  
 603 over a) SEA, b) WCE, c) SAS, and d) CNA region.

604  
 605

### 606 3.7 Model Effectiveness Across Seasons and Regions

607 Analysis of forecasts of extreme precipitation indices over all five models reveals that with  
 608 increase in the precipitation threshold the model's bias increases, suggesting a lack of skill in  
 609 modelling severe precipitation events. Correlation scores are lower in extratropical regions as  
 610 compared to the tropical regions, Likely due to the inherent unpredictability of extratropical  
 611 variability and model limitations in replicating land surface processes and tropical-  
 612 extratropical interactions, including the Pacific-South American (PSA) pattern and the  
 613 Pacific-North American (PNA) pattern, both of which can be influenced by ENSO and the  
 614 MJO (De Andrade et al., 2019). This is illustrated in Figure 10 where in the extratropical  
 615 regions models were unable to meet the selection criteria (i.e., having statistically significant  
 616 correlation while showing low bias) for most of the indices. This figure highlights the  
 617 superiority of UK-Met and Météo-France for all the four seasons. In the MAM, and JJA  
 618 season ECCC model has been selected frequently in some regions. The CMCC model is also  
 619 an effective model after UK-Met and Météo-France by showing higher skill than the rest of  
 620 models for a considerable number of indices and regions. The frequency of selecting each  
 621 model at each region and over the 28 climate indices is illustrated in the Figure S18. As an  
 622 example, in the MAM season at the SEA region for 10 of the indices Météo-France model is  
 623 selected as a superior model (i.e., having significant correlation while a lower bias compared  
 624 to other models). For the SON season UK-Met model is the superior model over most of the  
 625 indices. Another noteworthy example would be NSA region where combination of UK-Met  
 626 and CMCC models are skilful in predicting extreme events. In MAM season UK-Met meets  
 627 the selection criteria for 13 of the indices and CMCC pass the selection criteria for 9 of the

628 indices. In the JJA season UK-Met model meets the selection criteria for 13 of the indices  
 629 while during DJF season the CMCC meets the selection criteria for 12 of the indices.

630

631 Over the SON season, UK-Met meet the selection criteria for 12 indices and CMCC for 7 of  
 632 the remaining indices. It is evident that using these two models over NSA region provides the  
 633 ability to capture large portion of extreme events. These results highlight the effectiveness of  
 634 our impact-based framework in capturing variety of extreme climatic events by combination  
 635 of different models in different season.

636

637

638

639

640

641

642

643

644

645

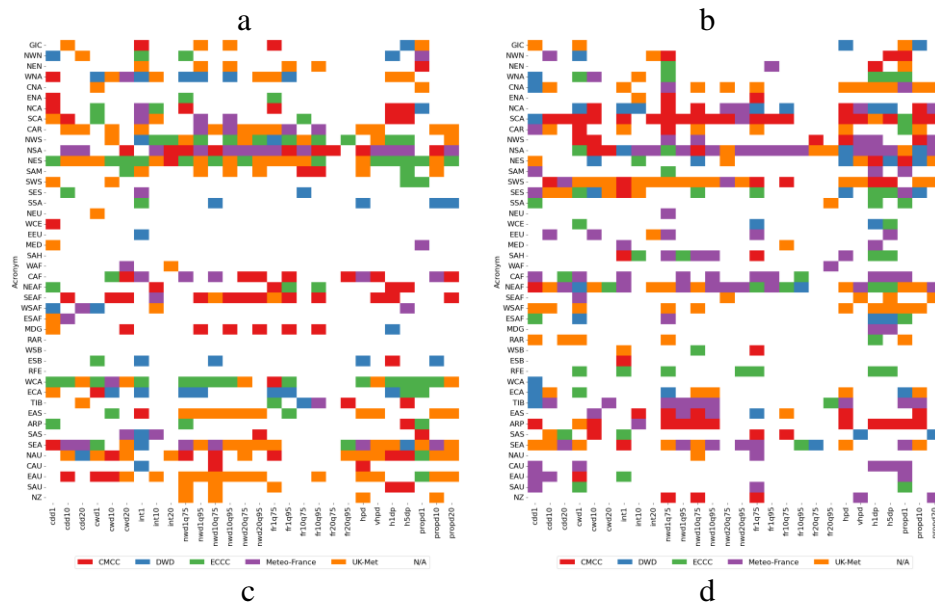
646

647

648

649

650





682 We develop an impact-based framework to assess the abilities of climate models in detecting  
683 extreme events in regions susceptible to cascading natural disasters like wildfires and floods.  
684 To evaluate performance in areas prone to wildfires, we employed indices such as cdd1, and  
685 propd1. For flood-prone zones, we used nwd10q75 and hpd as primary indices.

686  
687 In the context of wildfire risk analysis, notable differences in predictive capacities are  
688 observed, with specific models showcasing their powers in different regions and for different  
689 extreme precipitation indices. In the Northern Australia region (NAU), Météo-France and  
690 ECCC models display robust performance in predicting consecutive dry days. In the Southern  
691 Africa region (SEAF), the DWD model emerged as a frontrunner for predicting extreme  
692 precipitation events. The UK-Met model shows promising results for Western North America  
693 (WNA). Lastly, the DWD model shows good performance for the North South America  
694 (NSA) region. The analysis reveals models' relative strengths and weaknesses in predicting  
695 various precipitation characteristics, providing valuable insights for wildfire-related risk  
696 assessments.

697  
698 For flood-prone regions, the UK-Met model demonstrates superior predictive capabilities in  
699 the South-East Asia (SEA) monsoon season (JJA), marked by high correlation and low bias.  
700 In Western and Central Europe during the flood season (DJF), the ECCC model excel with  
701 notable correlation and comparable bias, despite challenges in capturing reference data  
702 variations. In South Asia (SAS) during the JJA season, the UK-Met and CMCC models  
703 excel, with the UK-Met showing favourable correlation and low bias.

704  
705 Our analysis of extreme precipitation indices across multiple models reveals that higher  
706 precipitation thresholds correspond to increased model bias, indicating a lack of skill in  
707 modelling severe precipitation events. Lower correlation scores in extratropical regions can  
708 be attributed to the inherent unpredictability of extratropical variability and the errors  
709 stemming from model deficiencies in representing teleconnections (De Andrade et al., 2019).  
710 The superiority of UK-Met and Météo-France models throughout all four seasons is  
711 emphasized, with ECCC also performing well in specific regions. The ECCC and CMCC  
712 models demonstrate effectiveness, following UK-Met and Météo-France, across specific  
713 indices and regions. The combined use of models emerges as a successful approach for  
714 predicting extreme events across different seasons. These findings underscore the efficacy of  
715 the impact-based framework in comprehensively capturing a wide range of extreme climatic  
716 events through a strategic combination of diverse models across different seasons.

## 717 718 719 **Data Availability Statement**

720  
721 The data used in this study were obtained from the European Centre for Medium-Range  
722 Weather Forecasts (ECMWF) Copernicus Climate Change Service, specifically from the  
723 ERA5 reanalysis dataset and C3S seasonal forecasts. These datasets are publicly available  
724 through the Copernicus Climate Data Store (CDS) at <https://cds.climate.copernicus.eu> under  
725 an Open Data Commons Attribution 4.0 International (ODC-BY 4.0) license. To access the

726 data, users can register for a free account on the Copernicus Climate Data Store platform and  
727 follow the provided guidelines for data retrieval. The specific seasonal model version  
728 numbers used in this study are detailed in the Section 2 of the paper.

729

## 730 **References**

- 731 Abatzoglou, J. T., & Williams, A. P. (2016). Impact of anthropogenic climate change on  
732 wildfire across western US forests. *Proceedings of the National Academy of Sciences*,  
733 *113*(42), 11770–11775. <https://doi.org/10.1073/pnas.1607171113>
- 734 AghaKouchak, A., Huning, L. S., Chiang, F., Sadegh, M., Vahedifard, F., Mazdiyasn, O.,  
735 Moftakhari, H., & Mallakpour, I. (2018). How do natural hazards cascade to cause  
736 disasters? *Nature*, *561*(7724), 458–460. <https://doi.org/10.1038/d41586-018-06783-6>
- 737 AghaKouchak, A., Huning, L. S., Sadegh, M., Qin, Y., Markonis, Y., Vahedifard, F., Love,  
738 C. A., Mishra, A., Mehran, A., Obringer, R., Hjelmstad, A., Pallickara, S., Jiwa, S.,  
739 Hanel, M., Zhao, Y., Pendergrass, A. G., Arabi, M., Davis, S. J., Ward, P. J., ...  
740 Kreibich, H. (2023). Toward impact-based monitoring of drought and its cascading  
741 hazards. *Nature Reviews Earth & Environment*, *4*(8), 582–595.  
742 <https://doi.org/10.1038/s43017-023-00457-2>
- 743 Alfieri, L., Burek, P., Dutra, E., Krzeminski, B., Muraro, D., Thielen, J., & Pappenberger, F.  
744 (2013). GloFAS – global ensemble streamflow forecasting and flood early warning.  
745 *Hydrology and Earth System Sciences*, *17*(3), 1161–1175.  
746 <https://doi.org/10.5194/hess-17-1161-2013>
- 747 Alizadeh, M. R., Abatzoglou, J. T., Adamowski, J., Modaresi Rad, A., AghaKouchak, A.,  
748 Pausata, F. S. R., & Sadegh, M. (2023). Elevation-dependent intensification of fire  
749 danger in the western United States. *Nature Communications*, *14*(1), 1773.  
750 <https://doi.org/10.1038/s41467-023-37311-4>
- 751 Alizadeh, M. R., Abatzoglou, J. T., Luce, C. H., Adamowski, J. F., Farid, A., & Sadegh, M.  
752 (2021). Warming enabled upslope advance in western US forest fires. *Proceedings of*

753            *the National Academy of Sciences*, 118(22), e2009717118.  
754            <https://doi.org/10.1073/pnas.2009717118>

755    Arheimer, B., Pimentel, R., Isberg, K., Crochemore, L., Andersson, J. C. M., Hasan, A., &  
756            Pineda, L. (2020). Global catchment modelling using World-Wide HYPE (WWH),  
757            open data, and stepwise parameter estimation. *Hydrology and Earth System Sciences*,  
758            24(2), 535–559. <https://doi.org/10.5194/hess-24-535-2020>

759    *Assessment of Intraseasonal to Interannual Climate Prediction and Predictability* (p. 12878).  
760            (2010). National Academies Press. <https://doi.org/10.17226/12878>

761    Ávila, A., Justino, F., Wilson, A., Bromwich, D., & Amorim, M. (2016). Recent precipitation  
762            trends, flash floods and landslides in southern Brazil. *Environmental Research*  
763            *Letters*, 11(11), 114029. <https://doi.org/10.1088/1748-9326/11/11/114029>

764    Baldwin, M. P., Stephenson, D. B., Thompson, D. W. J., Dunkerton, T. J., Charlton, A. J., &  
765            O'Neill, A. (2003). Stratospheric Memory and Skill of Extended-Range Weather  
766            Forecasts. *Science*, 301(5633), 636–640. <https://doi.org/10.1126/science.1087143>

767    Becker, E., Den Dool, H. V., & Zhang, Q. (2014). Predictability and Forecast Skill in  
768            NMME. *Journal of Climate*, 27(15), 5891–5906. <https://doi.org/10.1175/JCLI-D-13->  
769            00597.1

770    Borovikov, A., Cullather, R., Kovach, R., Marshak, J., Vernieres, G., Vikhliaev, Y., Zhao, B.,  
771            & Li, Z. (2019). GEOS-5 seasonal forecast system. *Climate Dynamics*, 53(12), 7335–  
772            7361. <https://doi.org/10.1007/s00382-017-3835-2>

773    Chervenkov, H., & Slavov, K. (2019). STARDEX and ETCCDI Climate Indices Based on E-  
774            OBS and CARPATCLIM: Part Two: ClimData in Use. In G. Nikolov, N. Kolkovska,  
775            & K. Georgiev (Eds.), *Numerical Methods and Applications* (Vol. 11189, pp. 368–  
776            374). Springer International Publishing. <https://doi.org/10.1007/978-3-030-10692->  
777            8\_41

778 Chervenkov, H., Slavov, K., & Ivanov, V. (2019). STARDEX and ETCCDI Climate Indices  
779 Based on E-OBS and CARPATCLIM: Part One: General Description. In G. Nikolov,  
780 N. Kolkovska, & K. Georgiev (Eds.), *Numerical Methods and Applications* (Vol.  
781 11189, pp. 360–367). Springer International Publishing. [https://doi.org/10.1007/978-](https://doi.org/10.1007/978-3-030-10692-8_40)  
782 [3-030-10692-8\\_40](https://doi.org/10.1007/978-3-030-10692-8_40)

783 Chuvieco, E., Pettinari, M. L., Lizundia-Loiola, J., Storm, T., & Padilla Parellada, M. (2018).  
784 *ESA Fire Climate Change Initiative (Fire\_cci): MODIS Fire\_cci Burned Area Pixel*  
785 *product, version 5.1* (3.1) [Application/xml]. Centre for Environmental Data Analysis  
786 (CEDA). <https://doi.org/10.5285/58F00D8814064B79A0C49662AD3AF537>

787 Committee on Developing a U.S. Research Agenda to Advance Subseasonal to Seasonal  
788 Forecasting, Board on Atmospheric Sciences and Climate, Ocean Studies Board,  
789 Division on Earth and Life Studies, & National Academies of Sciences, Engineering,  
790 and Medicine. (2016). *Next Generation Earth System Prediction: Strategies for*  
791 *Subseasonal to Seasonal Forecasts* (p. 21873). National Academies Press.  
792 <https://doi.org/10.17226/21873>

793 De Andrade, F. M., Coelho, C. A. S., & Cavalcanti, I. F. A. (2019). Global precipitation  
794 hindcast quality assessment of the Subseasonal to Seasonal (S2S) prediction project  
795 models. *Climate Dynamics*, 52(9–10), 5451–5475. [https://doi.org/10.1007/s00382-](https://doi.org/10.1007/s00382-018-4457-z)  
796 [018-4457-z](https://doi.org/10.1007/s00382-018-4457-z)

797 Du, H., Donat, M. G., Zong, S., Alexander, L. V., Manzanas, R., Kruger, A., Choi, G.,  
798 Salinger, J., He, H. S., Li, M.-H., Fujibe, F., Nandintsetseg, B., Rehman, S., Abbas,  
799 F., Rusticucci, M., Srivastava, A., Zhai, P., Lippmann, T., Yabi, I., ... Wu, Z. (2022).  
800 Extreme Precipitation on Consecutive Days Occurs More Often in a Warming  
801 Climate. *Bulletin of the American Meteorological Society*, 103(4), E1130–E1145.  
802 <https://doi.org/10.1175/BAMS-D-21-0140.1>

803 Dunn, R. J. H., Donat, M. G., & Alexander, L. V. (2022). Comparing extremes indices in  
804 recent observational and reanalysis products. *Frontiers in Climate*, 4, 989505.  
805 <https://doi.org/10.3389/fclim.2022.989505>

806 Friedl, M., & Sulla-Menashe, D. (2022). *MODIS/Terra+Aqua Land Cover Type Yearly L3*  
807 *Global 500m SIN Grid V061* [dataset]. NASA EOSDIS Land Processes Distributed  
808 Active Archive Center. <https://doi.org/10.5067/MODIS/MCD12Q1.061>

809 García-Franco, J. L., Lee, C.-Y., Camargo, S. J., Tippet, M. K., Kim, D., Molod, A., & Lim,  
810 Y.-K. (2023). Climatology of tropical cyclone precipitation in the S2S models.  
811 *Weather and Forecasting*. <https://doi.org/10.1175/WAF-D-23-0029.1>

812 Gebrechorkos, S. H., Pan, M., Beck, H. E., & Sheffield, J. (2022). Performance of State-of-  
813 the-Art C3S European Seasonal Climate Forecast Models for Mean and Extreme  
814 Precipitation Over Africa. *Water Resources Research*, 58(3).  
815 <https://doi.org/10.1029/2021WR031480>

816 Giuntoli, I., Fabiano, F., & Corti, S. (2022). Seasonal predictability of Mediterranean weather  
817 regimes in the Copernicus C3S systems. *Climate Dynamics*, 58(7–8), 2131–2147.  
818 <https://doi.org/10.1007/s00382-021-05681-4>

819 Gong, P., Li, X., Wang, J., Bai, Y., Chen, B., Hu, T., Liu, X., Xu, B., Yang, J., Zhang, W., &  
820 Zhou, Y. (2020). Annual maps of global artificial impervious area (GAIA) between  
821 1985 and 2018. *Remote Sensing of Environment*, 236, 111510.  
822 <https://doi.org/10.1016/j.rse.2019.111510>

823 Guimarães, B. D. S., Coelho, C. A. D. S., Woolnough, S. J., Kubota, P. Y., Bastarz, C. F.,  
824 Figueroa, S. N., Bonatti, J. P., & De Souza, D. C. (2021). An inter-comparison  
825 performance assessment of a Brazilian global sub-seasonal prediction model against  
826 four sub-seasonal to seasonal (S2S) prediction project models. *Climate Dynamics*,  
827 56(7–8), 2359–2375. <https://doi.org/10.1007/s00382-020-05589-5>

828 Hao, Z., Singh, V. P., & Xia, Y. (2018). Seasonal Drought Prediction: Advances, Challenges,  
829 and Future Prospects. *Reviews of Geophysics*, *56*(1), 108–141.  
830 <https://doi.org/10.1002/2016RG000549>

831 Iturbide, M., Gutiérrez, J. M., Alves, L. M., Bedia, J., Cerezo-Mota, R., Gimadevilla, E.,  
832 Cofiño, A. S., Di Luca, A., Faria, S. H., Gorodetskaya, I. V., Hauser, M., Herrera, S.,  
833 Hennessy, K., Hewitt, H. T., Jones, R. G., Krakovska, S., Manzananas, R., Martínez-  
834 Castro, D., Narisma, G. T., ... Vera, C. S. (2020). An update of IPCC climate  
835 reference regions for subcontinental analysis of climate model data: Definition and  
836 aggregated datasets. *Earth System Science Data*, *12*(4), 2959–2970.  
837 <https://doi.org/10.5194/essd-12-2959-2020>

838 Jie, W., Vitart, F., Wu, T., & Liu, X. (2017). Simulations of the Asian summer monsoon in  
839 the sub-seasonal to seasonal prediction project (S2S) database: Simulations of Asian  
840 Summer Monsoon in the S2S Database. *Quarterly Journal of the Royal  
841 Meteorological Society*, *143*(706), 2282–2295. <https://doi.org/10.1002/qj.3085>

842 Khorshidi, M. S., Dennison, P. E., Nikoo, M. R., AghaKouchak, A., Luce, C. H., & Sadegh,  
843 M. (2020). Increasing concurrence of wildfire drivers tripled megafire critical danger  
844 days in Southern California between 1982 and 2018. *Environmental Research Letters*,  
845 *15*(10), 104002. <https://doi.org/10.1088/1748-9326/abae9e>

846 King, A. D., Hudson, D., Lim, E., Marshall, A. G., Hendon, H. H., Lane, T. P., & Alves, O.  
847 (2020). Sub-seasonal to seasonal prediction of rainfall extremes in Australia.  
848 *Quarterly Journal of the Royal Meteorological Society*, *146*(730), 2228–2249.  
849 <https://doi.org/10.1002/qj.3789>

850 Kumar, A., & Zhu, J. (2018). Spatial Variability in Seasonal Prediction Skill of SSTs:  
851 Inherent Predictability or Forecast Errors? *Journal of Climate*, *31*(2), 613–621.  
852 <https://doi.org/10.1175/JCLI-D-17-0279.1>

853 Lau, W. K.-M., & Waliser, D. E. (2012). *Intraseasonal Variability in the Atmosphere-Ocean*  
854 *Climate System*. Springer Berlin Heidelberg. <https://doi.org/10.1007/978-3-642->  
855 [13914-7](https://doi.org/10.1007/978-3-642-13914-7)

856 Lizundia-Loiola, J., Otón, G., Ramo, R., & Chuvieco, E. (2020). A spatio-temporal active-  
857 fire clustering approach for global burned area mapping at 250 m from MODIS data.  
858 *Remote Sensing of Environment*, 236, 111493.  
859 <https://doi.org/10.1016/j.rse.2019.111493>

860 Mallakpour, I., Sadeghi, M., Mosaffa, H., Akbari Asanjan, A., Sadegh, M., Nguyen, P.,  
861 Sorooshian, S., & AghaKouchak, A. (2022). Discrepancies in changes in precipitation  
862 characteristics over the contiguous United States based on six daily gridded  
863 precipitation datasets. *Weather and Climate Extremes*, 36, 100433.  
864 <https://doi.org/10.1016/j.wace.2022.100433>

865 Mandrekar, J. N. (2010). Receiver Operating Characteristic Curve in Diagnostic Test  
866 Assessment. *Journal of Thoracic Oncology*, 5(9), 1315–1316.  
867 <https://doi.org/10.1097/JTO.0b013e3181ec173d>

868 McAdam, R., Masina, S., Balmaseda, M., Gualdi, S., Senan, R., & Mayer, M. (2022).  
869 Seasonal forecast skill of upper-ocean heat content in coupled high-resolution  
870 systems. *Climate Dynamics*, 58(11–12), 3335–3350. <https://doi.org/10.1007/s00382->  
871 [021-06101-3](https://doi.org/10.1007/s00382-021-06101-3)

872 Modaresi Rad, A., Kreitler, J., Abatzoglou, J. T., Fallon, K., Roche, K. R., & Sadegh, M.  
873 (2022). Anthropogenic stressors compound climate impacts on inland lake dynamics:  
874 The case of Hamun Lakes. *Science of The Total Environment*, 829, 154419.  
875 <https://doi.org/10.1016/j.scitotenv.2022.154419>

876 Moron, V., & Robertson, A. W. (2020). Tropical rainfall subseasonal-to-seasonal  
877 predictability types. *Npj Climate and Atmospheric Science*, 3(1), 4.  
878 <https://doi.org/10.1038/s41612-020-0107-3>

879 Nobakht, M., Saghafian, B., & Aminyavari, S. (2021). Skill Assessment of Copernicus  
880 Climate Change Service Seasonal Ensemble Precipitation Forecasts over Iran.  
881 *Advances in Atmospheric Sciences*, 38(3), 504–521. [https://doi.org/10.1007/s00376-](https://doi.org/10.1007/s00376-020-0025-7)  
882 [020-0025-7](https://doi.org/10.1007/s00376-020-0025-7)

883 Rivoire, P., Martius, O., Naveau, P., & Tuel, A. (2023). Assessment of subseasonal-to-  
884 seasonal (S2S) ensemble extreme precipitation forecast skill over Europe. *Natural*  
885 *Hazards and Earth System Sciences*, 23(8), 2857–2871. [https://doi.org/10.5194/nhess-](https://doi.org/10.5194/nhess-23-2857-2023)  
886 [23-2857-2023](https://doi.org/10.5194/nhess-23-2857-2023)

887 Roy, T., He, X., Lin, P., Beck, H. E., Castro, C., & Wood, E. F. (2020). Global Evaluation of  
888 Seasonal Precipitation and Temperature Forecasts from NMME. *Journal of*  
889 *Hydrometeorology*, 21(11), 2473–2486. <https://doi.org/10.1175/JHM-D-19-0095.1>

890 Sadegh, M., Moftakhari, H., Gupta, H. V., Ragno, E., Mazdidasni, O., Sanders, B., Matthew,  
891 R., & AghaKouchak, A. (2018). Multihazard Scenarios for Analysis of Compound  
892 Extreme Events. *Geophysical Research Letters*, 45(11), 5470–5480.  
893 <https://doi.org/10.1029/2018GL077317>

894 Samaniego, L., Thober, S., Wanders, N., Pan, M., Rakovec, O., Sheffield, J., Wood, E. F.,  
895 Prudhomme, C., Rees, G., Houghton-Carr, H., Fry, M., Smith, K., Watts, G., Hisdal,  
896 H., Estrela, T., Buontempo, C., Marx, A., & Kumar, R. (2019). Hydrological  
897 Forecasts and Projections for Improved Decision-Making in the Water Sector in  
898 Europe. *Bulletin of the American Meteorological Society*, 100(12), 2451–2472.  
899 <https://doi.org/10.1175/BAMS-D-17-0274.1>

900 Schiavina, M., Freire, S., & MacManus, K. (2023). *GHS-POP R2023A - GHS population*  
901 *grid multitemporal (1975-2030)* [dataset]. European Commission, Joint Research  
902 Centre (JRC). <https://doi.org/10.2905/2FF68A52-5B5B-4A22-8F40-C41DA8332CFE>

903 Sen, P. K. (1968). Estimates of the Regression Coefficient Based on Kendall's Tau. *Journal*  
904 *of the American Statistical Association*, 63(324), 1379–1389.  
905 <https://doi.org/10.1080/01621459.1968.10480934>

906 Sharma, A. R., Jain, P., Abatzoglou, J. T., & Flannigan, M. (2022). Persistent Positive  
907 Anomalies in Geopotential Heights Promote Wildfires in Western North America.  
908 *Journal of Climate*, 35(19), 6469–6486. <https://doi.org/10.1175/JCLI-D-21-0926.1>

909 Shukla, J., Marx, L., Paolino, D., Straus, D., Anderson, J., Ploshay, J., Baumhefner, D.,  
910 Tribbia, J., Brankovic, C., Palmer, T., Chang, Y., Schubert, S., Suarez, M., & Kalnay,  
911 E. (2000). Dynamical Seasonal Prediction. *Bulletin of the American Meteorological*  
912 *Society*, 81(11), 2593–2606. [https://doi.org/10.1175/1520-](https://doi.org/10.1175/1520-0477(2000)081<2593:DSP>2.3.CO;2)  
913 [0477\(2000\)081<2593:DSP>2.3.CO;2](https://doi.org/10.1175/1520-0477(2000)081<2593:DSP>2.3.CO;2)

914 Tapiador, F. J., Roca, R., Del Genio, A., Dewitte, B., Petersen, W., & Zhang, F. (2019). Is  
915 Precipitation a Good Metric for Model Performance? *Bulletin of the American*  
916 *Meteorological Society*, 100(2), 223–233. [https://doi.org/10.1175/BAMS-D-17-](https://doi.org/10.1175/BAMS-D-17-0218.1)  
917 [0218.1](https://doi.org/10.1175/BAMS-D-17-0218.1)

918 Tellman, B., Sullivan, J. A., Kuhn, C., Kettner, A. J., Doyle, C. S., Brakenridge, G. R.,  
919 Erickson, T. A., & Slayback, D. A. (2021). Satellite imaging reveals increased  
920 proportion of population exposed to floods. *Nature*, 596(7870), 80–86.  
921 <https://doi.org/10.1038/s41586-021-03695-w>

922 Thielen, J., Bartholmes, J., Ramos, M.-H., & De Roo, A. (2009). The European Flood Alert  
923 System – Part 1: Concept and development. *Hydrology and Earth System Sciences*,  
924 *13*(2), 125–140. <https://doi.org/10.5194/hess-13-125-2009>

925 Turco, M., Abatzoglou, J. T., Herrera, S., Zhuang, Y., Jerez, S., Lucas, D. D., AghaKouchak,  
926 A., & Cvijanovic, I. (2023). Anthropogenic climate change impacts exacerbate  
927 summer forest fires in California. *Proceedings of the National Academy of Sciences*,  
928 *120*(25), e2213815120. <https://doi.org/10.1073/pnas.2213815120>

929 Villarini, G., Vecchi, G. A., Knutson, T. R., Zhao, M., & Smith, J. A. (2011). North Atlantic  
930 Tropical Storm Frequency Response to Anthropogenic Forcing: Projections and  
931 Sources of Uncertainty. *Journal of Climate*, *24*(13), 3224–3238.  
932 <https://doi.org/10.1175/2011JCLI3853.1>

933 Vitart, F., Ardilouze, C., Bonet, A., Brookshaw, A., Chen, M., Codorean, C., Déqué, M.,  
934 Ferranti, L., Fucile, E., Fuentes, M., Hendon, H., Hodgson, J., Kang, H.-S., Kumar,  
935 A., Lin, H., Liu, G., Liu, X., Malguzzi, P., Mallas, I., ... Zhang, L. (2017). The  
936 Subseasonal to Seasonal (S2S) Prediction Project Database. *Bulletin of the American*  
937 *Meteorological Society*, *98*(1), 163–173. <https://doi.org/10.1175/BAMS-D-16-0017.1>

938 Vitart, F., & Robertson, A. W. (2018). The sub-seasonal to seasonal prediction project (S2S)  
939 and the prediction of extreme events. *Npj Climate and Atmospheric Science*, *1*(1), 3.  
940 <https://doi.org/10.1038/s41612-018-0013-0>

941 Wanders, N., & Wood, E. F. (2016). Improved sub-seasonal meteorological forecast skill  
942 using weighted multi-model ensemble simulations. *Environmental Research Letters*,  
943 *11*(9), 094007. <https://doi.org/10.1088/1748-9326/11/9/094007>

944 Wanthanaporn, U., Supit, I., Van Hove, B., & Hutjes, R. W. A. (2023). *Analysis of seasonal*  
945 *climate and streamflow forecasts performance for Mainland Southeast Asia*  
946 [Preprint]. Water Resources Management/Modelling approaches.  
947 <https://doi.org/10.5194/hess-2023-56>

948 Xu, L., Chen, N., Chen, Z., Zhang, C., & Yu, H. (2021). Spatiotemporal forecasting in earth  
949 system science: Methods, uncertainties, predictability and future directions. *Earth-*  
950 *Science Reviews*, 222, 103828. <https://doi.org/10.1016/j.earscirev.2021.103828>

951 Xue, P., Malanotte-Rizzoli, P., Wei, J., & Eltahir, E. A. B. (2020). Coupled Ocean-  
952 Atmosphere Modeling Over the Maritime Continent: A Review. *Journal of*  
953 *Geophysical Research: Oceans*, 125(6). <https://doi.org/10.1029/2019JC014978>

954 Zhang, Y., Wallace, J. M., & Battisti, D. S. (1997). ENSO-like Interdecadal Variability:  
955 1900–93. *Journal of Climate*, 10(5), 1004–1020. [https://doi.org/10.1175/1520-](https://doi.org/10.1175/1520-0442(1997)010<1004:ELIV>2.0.CO;2)  
956 [0442\(1997\)010<1004:ELIV>2.0.CO;2](https://doi.org/10.1175/1520-0442(1997)010<1004:ELIV>2.0.CO;2)

957 Zhou, Y., Zaitchik, B. F., Kumar, S. V., Arsenault, K. R., Matin, M. A., Qamer, F. M.,  
958 Zamora, R. A., & Shakya, K. (2021). Developing a hydrological monitoring and sub-  
959 seasonal to seasonal forecasting system for South and Southeast Asian river basins.  
960 *Hydrology and Earth System Sciences*, 25(1), 41–61. [https://doi.org/10.5194/hess-25-](https://doi.org/10.5194/hess-25-41-2021)  
961 [41-2021](https://doi.org/10.5194/hess-25-41-2021)

962

963